Strain-induced formation of self-assembled InGaN/GaN superlattices in nominal InGaN films grown by plasma-assisted molecular beam epitaxy

Kamruzzaman Khan,[1] Kai Sun,[1] Christian Wurm,[2] Kanak Datta,[3] Parag B. Deotare,[3,4] and Elaheh Ahmadi[3,4,*]

[1]*Department of Materials Science and Engineering, University of Michigan, Ann Arbor, Michigan 48109, USA*
[2]*Department of Electrical and Computer Engineering, University of California Santa Barbara, California 93106, USA*
[3]*Department of Electrical Engineering and Computer Science, University of Michigan, Ann Arbor, Michigan 48109, USA*
[4]*Applied Physics Program, University of Michigan, Ann Arbor, Michigan 48109, USA*

(Received 16 July 2021; accepted 22 November 2021; published 28 December 2021)

In this work, we report the spontaneous formation of superlattice structures in nominal InGaN films grown by plasma-assisted molecular beam epitaxy. A 700-nm-thick self-assembled $In_{0.2}Ga_{0.8}N$/GaN superlattice with excellent structural quality was achieved. Strain was studied as a possible driving force for the formation of self-assembled superlattice (SASL) structure by growth of InGaN on ZnO substrate using similar growth conditions. The SASL structures were optically characterized using photoluminescence spectroscopy. Structural characterization was conducted via transmission electron microscopy and atom probe tomography. High-resolution x-ray diffraction (XRD) and XRD reciprocal space map were utilized to determine the average composition and the degree of relaxation of InGaN films. We propose that the vertical phase separation observed in the SASL structure is caused by high-temperature growth and intensified by strain. This work provides a method for engineering strain and growth of thick InGaN films for a variety of applications including solar cells and photodetectors.

DOI: 10.1103/PhysRevMaterials.5.124606

I. INTRODUCTION

The InGaN alloy system is attractive for a variety of optoelectronic applications, including laser diodes [1–3], light-emitting diodes [4–6], and photodetectors [7,8], as it enables direct band-gap tuning within a large range (0.7–3.4 eV). The (In,Ga)N material system is also attractive for photovoltaic applications as its optical absorption covers the solar spectrum [9–12]. Thick InGaN films (several hundred nanometers thick) with InN mole fraction larger than 10% are required for this purpose. However, the growth of high In-content InGaN films remains challenging due to 10% lattice mismatch and large thermal stability difference between InN and GaN [13–18]. InGaN films can be grown pseudomorphically on GaN below a critical thickness, which reduces sharply as the InN mole fraction in InGaN increases due to the lattice mismatch between InN and GaN [15,19]. As the thickness increases beyond the critical thickness, InGaN film relaxes to relieve the strain via formation of defects and dislocations [20–28].

In 2011, It was shown [29] that using a high growth rate ($\sim$1.3 μm/h) in plasma-assisted molecular beam epitaxy (PAMBE) can enhance the structural quality of 350-nm-thick InGaN films with an average 10% In content compared with those grown using a conventional growth rate ($\sim$360 nm/h). In this study, a self-assembled superlattice (SASL) structure was observed in the faster-grown sample. The superior structural quality of the fast-grown sample was attributed to the surface roughness suppression caused by kinetic limitation, and the inhibition of the Frank-Read dislocation generation mechanism within the spontaneously formed superlattice (SL) structure. The SASL structure observed in this work was composed of two monolayers and four monolayers of InGaN films with different In contents; however, the In content in each layer was not determined.

SASL structures formed by chemical ordering have been widely reported in ternary and quaternary conventional III–V semiconductors [30,31], and have been also observed in AlGaN and InGaN [32–34]. Northrup *et al.* [35,36] proposed that chemical ordering observed in InGaN alloys is because In atoms preferably incorporate at step edges [$(10\bar{1}1)$ microfacets] during growth on Ga-polar or N-polar surfaces. While most of the reported SASL structures are formed by chemical ordering [32,33], there have been only a few reports on the formation of SASL structure by phase separation [30,37,38]. Zheng *et al.* [38] observed composition modulation in a graded InGaN film grown by MBE. However, the modulation was irregular, weakened as the thickness increased beyond 100 nm and eventually vanished.

In this work, in contrast, we report on 700-nm-thick nominal "InGaN" film composed of a spontaneously formed SL structure made of 3-nm-thick $In_{0.2}Ga_{0.8}N$/3-nm-thick GaN layers. This allowed us to grow 700-nm-thick InGaN with an average InN mole fraction of $\sim$8% with excellent structural quality. Using similar growth conditions, InGaN was also grown on a ZnO substrate, which is in-plane lattice matched to $In_{0.2}Ga_{0.8}N$. The nominal InGaN films grown on GaN and ZnO were structurally characterized to investigate the impact of strain on the formation of SASL structure. We propose that the vertical phase separation observed in the SASL structure is caused by high-temperature growth and intensified by strain.

*eahmadi@umich.edu

II. EXPERIMENTAL METHODS

A. Epitaxial growth

All samples were grown in a Veeco GENxplor MBE system equipped with conventional Al, Ga, and In effusion cells and a radio-frequency (rf) plasma source to supply active nitrogen. The N source consisted of ultrahigh-purity (99.9995%) N_2 gas flowing at 1 SCCM through the rf-plasma source with 350-W rf power, which corresponded to a growth rate of 6 nm/min for metal-rich GaN layers. To ensure uniform temperature during the growth, 500-nm-thick Ti was deposited on the back side of the substrate via e-beam evaporation. The substrates were first solvent cleaned (acetone, methanol, and isopropanol for 4 min each) to remove organic residues from the surface, and then mounted on a Si substrate by In bonding before being loaded in the MBE exit-entry chamber. An hour of baking was performed at 400 °C in a buffer chamber to remove any water prior to transferring the substrate to the growth chamber. During the growth, the substrate temperature was measured and monitored using a thermocouple. The growth was monitored *in situ* via reflection high-energy electron diffraction (RHEED).

For growth on GaN, 1 cm × 1cm Ga-polar GaN-on-sapphire templates were used. The growth was initiated with a 200-nm-thick GaN in metal-rich growth regime at 730 °C using a Ga beam equivalent pressure of 3.8×10^{-7} Torr to ensure a smooth and clean surface. The excess Ga was desorbed every 20 min by closing the Ga shutter while keeping the nitrogen shutter open for 40 s [13,39]. The substrate temperature was then reduced to 600 °C, and growth was interrupted for 15 min to stabilize the substrate temperature. A 700-nm-thick InGaN film was then grown on sample A in In-rich growth regime using Ga and In fluxes of 3×10^{-7} and 1.7×10^{-7} Torr, respectively. It is worth noting that several InGaN samples were first grown to optimize In and Ga fluxes to achieve smooth surface morphology prior to the growth of samples discussed here. The *in situ* RHEED pattern on sample A is streaky, indicating an atomically smooth surface [see Appendix A, Fig. 6(a)].

For growth on ZnO, commercial 1 cm × 1 cm O-face ZnO (0001) substrates grown by the hydrothermal method were used. A UV ozone treatment followed by annealing of the substrate at 1050 °C was performed on ZnO substrates to obtain atomically smooth surface morphology with step edges. The details of substrate pretreatment can be found elsewhere [40]. The growth of sample B was initiated with the growth of ∼2-ML-thick low-temperature GaN at 440 °C by metal-enhanced epitaxy (MEE) to suppress chemical reaction between In/Ga adatoms with ZnO substrate and formation of a poor-quality interfacial oxide layer. More details about this can be found in Ref. [40]. The substrate temperature was then increased to 600 °C and growth was interrupted for 15 min to ensure the substrate temperature was stabilized. Then, 1-μm-thick InGaN was subsequently grown using In and Ga fluxes similar to those used for sample A. Several InGaN calibration samples on ZnO substrates were first grown to optimize In and Ga fluxes to achieve smooth surface morphology prior to the growth of sample discussed here. Sample B shows streaky RHEED pattern after growth as well which indicates atomically smooth surface [see Appendix A, Fig. 6(b)].

B. Structural characterization

A Bruker NanoMan atomic force microscopy (AFM) was employed to characterize the surface morphology of the samples. High-resolution x-ray diffraction (HRXRD) ω-2θ scans and (ω-2θ)-ω reciprocal space maps (RSM) were recorded on a triple-axis Philips X'pertPro Panalytical Pixel 3D materials research diffractometer. Cross-sectional specimens for transmission electron microscopy (TEM) study were prepared by *in situ* focused ion beam (FIB) lift-out methods using a Thermo-Fisher G4 650 Xe Plasma-FIB (P-FIB). Utilizing a Xe plasma ion source instead of a regular Ga source prevents redistribution of Ga atoms or change of Ga concentration in InGaN films. For final thinning, a 5-keV energy and 10-pA current beam were used. Needlelike cross-sectional specimen for atom probe tomography (APT) were also made using the same P-FIB. A JEOL JEM-3100R05 electron microscope with a cold-field emission gun equipped with both a probe and an imaging corrector was used for atom-resolved imaging that was operated in scanning transmission electron microscopy (STEM) mode. Both high-angle annular dark-field (HAADF) and bright-field images were taken simultaneously.

C. Optical characterization

The lateral composition uniformity of InGaN was characterized by employing steady-state and time resolved photoluminescence (PL) spectroscopy setup. The samples were excited with a diffraction-limited spot using 405-nm pulsed laser (∼30-ps pulse width, 40-MHz repetition rate) at room temperature using 60 × 0.95 numerical aperture dry objective (NIKON CFI PLAN APO λ 60X/0.95). For steady-state PL the sample emission was analyzed using a high-resolution spectrometer (Princeton Instruments IsoPlane SCT 320) coupled to a highly sensitive charge-coupled device camera (Princeton Instruments Pixis: 400). The slit width at the spectrometer entrance was kept at 250 μm with the spectrometer integration time set to 1.0 s. The PL scans were performed by keeping the laser excitation spot at a fixed position and scanning the sample by a piezo-nanopositioner stage in ∼200-nm steps. For time-resolved photoluminescence measurement, the sample emission was collected using a highly sensitive avalanche photodiode (APD) [Micro Photon Devices (MPD) Photon Detector Module (PDM) series]. The output of the APD was analyzed with a timing module (PicoQuant HydraHarp 400) synchronized to the laser diode module.

III. RESULTS AND DISCUSSION

AFM images of samples A and B are shown in Fig. 1. A relatively smooth surface (for such thick InGaN films) with root-mean-square (rms) roughness of ∼3 and 4.45 nm were measured on sample A and B, respectively. However, the density of spiral hillocks, which are associated with mixed (edge and screw) and screw threading dislocations [41], increased significantly on InGaN film grown on ZnO, indicating an increase in the threading dislocation density (TDD). A higher TDD in sample B could be due to formation of a low-quality interfacial layer due to chemical reaction between In or Ga atoms with ZnO. As mentioned earlier, the growth of sample B was initiated with the growth of ∼2-ML-thick

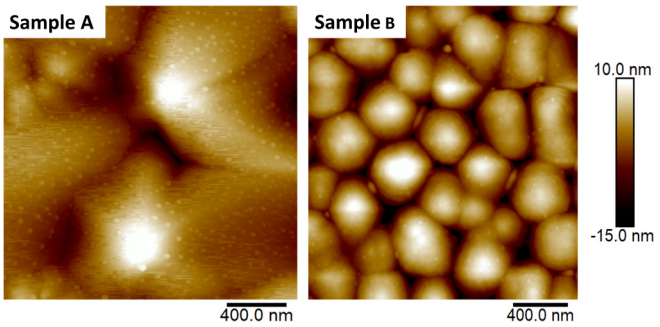

FIG. 1. A 2 × 2-μm^2 AFM image of samples A and B showing rms roughness of ∼3 and 4.45 nm, respectively.

low-temperature GaN at 440 °C by MEE to suppress this chemical reaction. However, 2-ML GaN may not be thick enough to fully cover the ZnO surface, leading to regions with poor-quality interfacial layer and consequently high density of threading dislocations.

A superlattice structure on the nominal InGaN film grown on sample A is evident from STEM-HAADF images shown in Figs. 2(a)–2(c). Three distinctive layers can be observed from the high-resolution STEM image taken from the region close to the GaN-InGaN interface [Fig. 2(c)]: (i) an ∼10-nm-thick InGaN layer, followed by (ii) an ∼17-nm-thick GaN layer, followed by (iii) a superlattice structure for the remaining of the growth. It is important to emphasize that all shutters were kept open, and fluxes were not changed during the 2-h growth of the InGaN film. We did not observe any fluctuations in the Ga/In effusion cells and substrate temperatures. The substrate temperature was monitored during the growth using a thermocouple. Additionally, the interface abruptness observed from STEM-HAADF images from this sample rules out temperature fluctuations as the cause for the formation of the SL structure. This suggests that the formation of the superlattice structure by In composition modulation is via a self-assembling process. Figure 2(a) also reveals that the SASL structure has a high structural quality with no newly generated dislocations or structural defects in this layer. STEM-HAADF image was also recorded over a larger area which showed a sharp interface and InGaN/GaN SL structure with high structural quality as well (see Appendix B, Fig. 7).

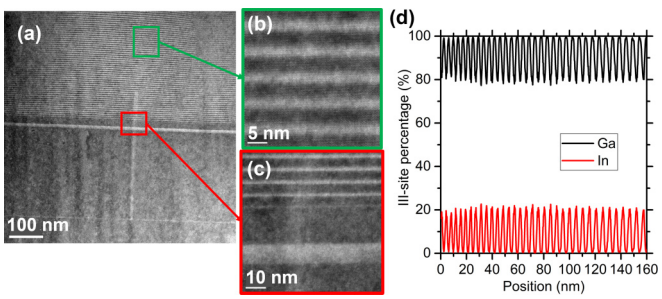

FIG. 2. (a) STEM-HAADF image of sample A, (b) showing SASL structure, and (c) magnified STEM-HAADF image of sample A near the interface with GaN showing three distinctive regions of (i) InGaN film, (ii) GaN layer, and (iii) layer with a superlattice structure. (d) In and Ga concentration profiles measured by APT showing a periodic variation of In content from 0 to 20%.

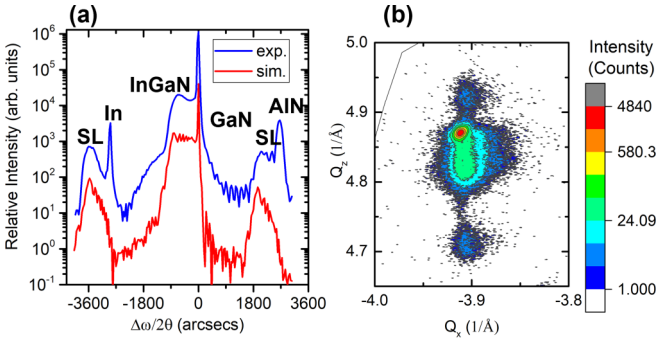

FIG. 3. (a) XRD ω-2θ scan around GaN (0002) reflection and (b) XRD-RSM scan around GaN ($\bar{1}\bar{1}$4) reflection recorded on sample A.

To quantify In content in the SL structure observed on sample A, APT was performed and In, Ga, and N concentrations were recorded and are demonstrated in Fig. 2(d). A periodic variation in In content from 0 to 20% was determined by APT.

XRD ω-2θ scan around GaN (0002) reflection was recorded on sample A and is shown in Fig. 3(a). The AlN peak observed in the XRD ω-2θ scan of sample A corresponds to the AlN nucleation layer in the GaN-on-sapphire template purchased commercially. XRD ω-2θ scan of the template shows similar AlN peak. The In peak is due to excess In accumulated on the surface which has been commonly observed on InGaN films grown in In-rich regime by PAMBE [42]. XRD ω-2θ profile of sample A suggests a graded InGaN film with the layer peak corresponding to an InGaN film with an average In content of ∼8%. It is important to note that only the average In content can be determined from the XRD measurement. Therefore, a "graded composition" observed in the XRD ω-2θ scan could be due to an increase in In content, an increase in the thickness of InGaN well, or a decrease in the thickness of the GaN barrier. As an example, the red profile shown in Fig. 3(a) was simulated assuming a 3-nm-thick InGaN/3-nm-thick GaN superlattice with In content in the InGaN layer increasing from 2 to 18% which matches closely with the experimental data and is consistent with the InN mole fraction measured by APT on the top 160 nm of the SL.

If the formation of SASL structures presented here were due to ordering, one would expect to see extra diffraction spots

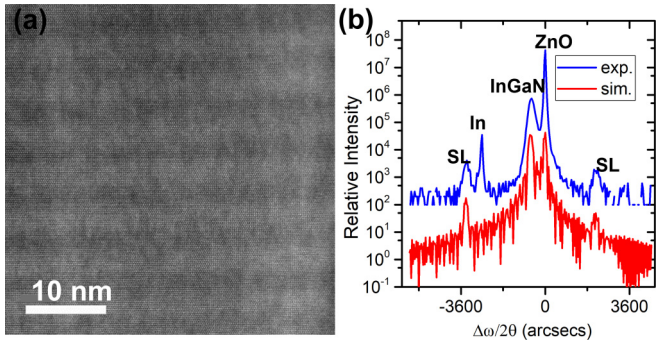

FIG. 4. (a) STEM-HAADF image of InGaN film grown on ZnO. (b) HRXRD ω-2θ scans of InGaN on ZnO substrate around ZnO (0002) reflection showing $In_{0.19}Ga_{0.81}N$ (3nm)/$In_{0.23}Ga_{0.87}N$ (3 nm) superlattice.

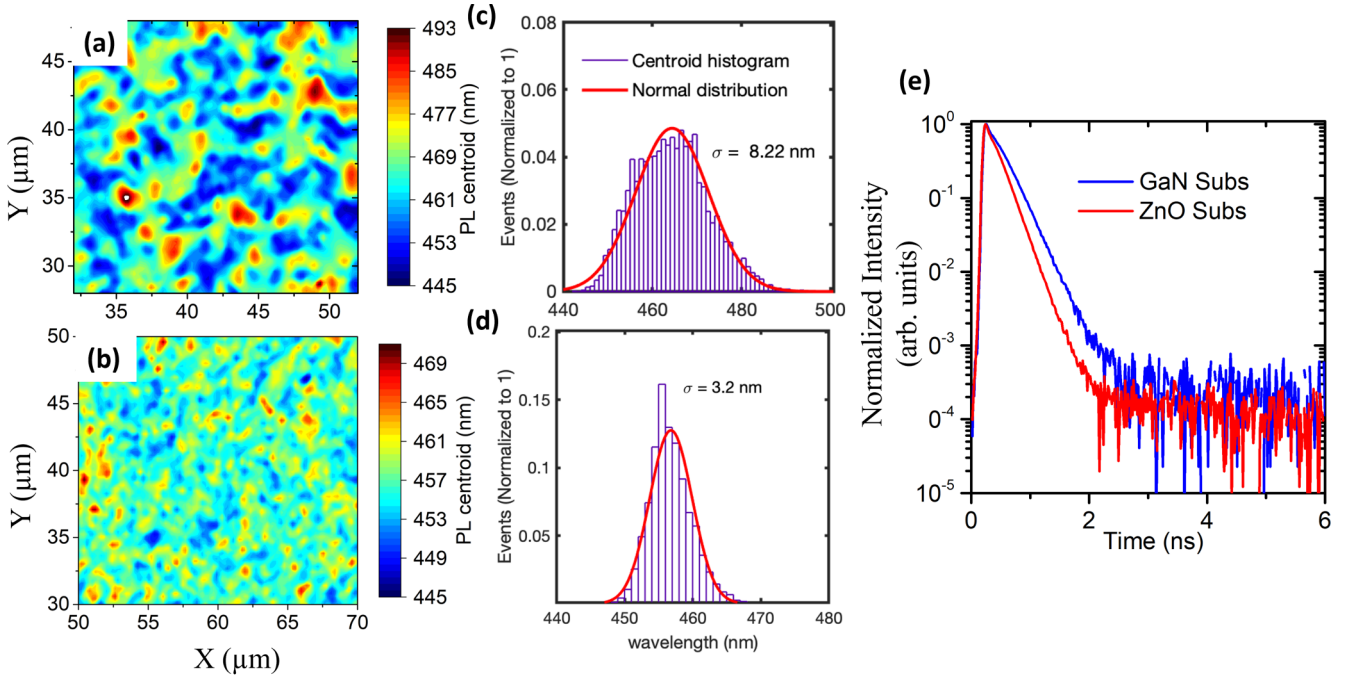

FIG. 5. PL intensity map of SASL structures grown on (a) GaN and (b) ZnO and histogram plot of PL mapping of SASL structures grown on (c) GaN and (d) ZnO. (e) Time-resolved PL of the SASL structures grown on GaN and ZnO.

or strike lines in the selected area electron diffraction (SAED) pattern [43,44]. However, the high-resolution STEM-HAADF and APT data taken on sample A (Fig. 2) have shown that there is no indium ordering except the formation of the superlattice. Also, the SAED pattern recorded on sample A (see Appendix C, Fig. 8) only has very sharp ordered diffraction spots from the crystal, suggesting that InGaN layers in the SASL structure are not ordered laterally. Our results also indicate that the SASL structure presented in this paper forms only in InGaN films grown at higher temperatures. For instance, the SASL was absent in the InGaN film grown at 560 °C (see Appendix D, Fig. 9). This observation suggests that the formation of the SASL structure may be due to vertical phase separation at higher growth temperatures.

XRD-RSM scan around GaN $(\bar{1}\bar{1}4)$ reflection was also recorded on sample A and is shown in Fig. 3(b). The RSM data indicate that the 700-nm-thick InGaN film with an average 8% In content is only 12% relaxed. This is three times thicker than the critical thickness of $In_{0.08}Ga_{0.92}N$ and so significantly higher amount of relaxation through formation of defects is expected [19,45,46]. This suggests that the formation of a self-assembled InGaN/GaN superlattice structure helps in managing the strain due to large lattice mismatch between InGaN and GaN, and consequently, leads to an enhancement in the critical thickness of InGaN film grown on GaN. Slight relaxation could be due to an increase in the height of hillocks as the InGaN thickness increases during the growth and therefore local elastic relaxation due to a 3D morphology can occur similar to what happens in nanowires [47,48]. The lateral widening of the RSM [shown in Fig. 3(b)] can be related to different In incorporation on the facets of hillocks compared with that on the c plane or asymmetric strain relaxation similar to that observed in nanowire [48].

The STEM-HAADF was also recorded on sample B [Fig. 4(a)] and revealed a SASL structure on the nominal InGaN film grown on ZnO. However, there is significantly less compositional modulation between the layers of SASL structure formed on InGaN film grown on ZnO (sample B) compared with that grown on GaN (sample A). The superlattice peaks are also visible in the HRXRD ω-2θ scan on sample B shown in Fig. 4(b). Simulations conducted using EPITAXY and SMOOTHFIT software revealed a good fit between the HRXRD ω-2θ profile with $In_{0.19}Ga_{0.81}N$ (3 nm)/$In_{0.23}Ga_{0.87}N$ (3 nm) superlattice structures, which is also consistent with the small compositional modulation observed in STEM image [Fig. 4(a)].

It is worth noting that although SASL structure can be observed on both samples, the In-content modulation in sample A is from 0 to 20%, whereas there is only a small variation (19 to 23%) in the In content of SASL structure grown on ZnO. While there is ∼2.2% lattice mismatch between $In_{0.2}Ga_{0.8}N$ and GaN, $In_{0.2}Ga_{0.8}N$ is in-plane lattice matched to ZnO. This indicates that the compressive strain built up in the InGaN film grown on GaN intensifies the vertical phase separation and the formation of SASL structure is a natural way for the system to manage the strain. Consequently, 700-nm-thick InGaN film with an average In content of 8% with high structural quality can be grown on GaN, which is several times larger than the critical thickness of $In_{0.08}Ga_{0.92}N$.

PL maps were measured over a 20 × 20-μm^2 area on the SASL structures grown on GaN (sample A) and ZnO (sample B) and are presented in Figs. 5(a) and 5(b) along with the histograms of PL centroid [Figs. 5(c) and 5(d)]. The histogram shows the normalized number of events (pixels) at a specific wavelength. The scale on PL maps is varied to illustrate the lateral wavelength variation in each sample more clearly. Both samples are relatively uniform. The centroid histogram can be fitted with a unimodal bell-shaped distribution with the center wavelength and variance of 460 and 8.2 nm for sample A and 456 and 3.2 nm for sample B. A slight lateral variation in the

peak wavelength is due to lateral fluctuations in the InGaN composition [49–53]. Additionally, as shown by Takeguchi *et al.* [51] in InGaN/GaN quantum wells, the band structure of the quantum well changes not only by quantum dot effects but also by the additional modulation of the internal polarization electric field. However, the polarization field in $In_{0.19}Ga_{0.81}N/In_{0.23}Ga_{0.77}N$ quantum wells grown on ZnO is expected to be significantly smaller than the polarization field in $In_{0.2}Ga_{0.8}N/GaN$ quantum wells grown coherently strained to GaN. Therefore, the wavelength broadening due to fluctuations in the internal electric field is expected to be significantly less in quantum wells grown on ZnO. Figure 5(e) shows time-resolved PL measurements on SASL grown on GaN and on ZnO. A slightly larger carrier lifetime was measured on SASL grown on GaN which is most probably due to less density of threading dislocations on this sample as revealed by AFM image [54] (Fig. 1). Besides, internal polarization electric field in SL resulting from quantum well width and In incorporation can affect the carrier lifetime [55,56]. Polarization field in $In_{0.2}Ga_{0.8}N/GaN$ SL strained to GaN is higher than that in $In_{0.19}Ga_{0.81}N/In_{0.23}Ga_{0.77}N$ SL grown on ZnO which can also lead to a higher carrier lifetime in sample A.

IV. CONCLUSION

In summary, we observed spontaneous formation of $In_{0.2}Ga_{0.8}N/GaN$ superlattice structure on nominal InGaN film grown on GaN by PAMBE. We studied the impact of strain on the superlattice formation by growing InGaN on ZnO using similar growth conditions. The self-assembled superlattice grown on ZnO showed less modulation in the In incorporation. Additionally, InGaN films grown at lower temperatures (e.g., 560 °C) did not show any superlattice structure. These observations suggest that the self-assembled superlattice structure may be due to vertical phase separation of InGaN caused by high-temperature growth and intensified by strain.

ACKNOWLEDGMENTS

The authors acknowledge funding support (Award No. N00014-18-1-2703) from the Office of Naval Research (Dr. Paul Maki, Program Manager). P.B.D. acknowledges support from National Science Foundation (NSF) Grant No. DMR-1904541. This work was partially performed using Lurie Nano Fabrication (LNF) facilities at the University of Michigan, Ann Arbor. The authors also acknowledge the financial support of the University of Michigan College of Engineering for the Thermo-Fisher G4 650 Xe Plasma-FIB and the financial support of the University of Michigan College of Engineering and NSF Grant No. MR-0723032 for the JEM-3100R05 and technical support from the Michigan Center for Materials Characterization. The authors thank Dr. Mahitosh Biswas for conducting the AFM measurement on samples grown on ZnO.

APPENDIX A

Streaky RHEED patterns were observed at the end of growth on both samples A and B as shown in Figs. 6(a) and 6(b), respectively, which indicates atomically smooth surface.

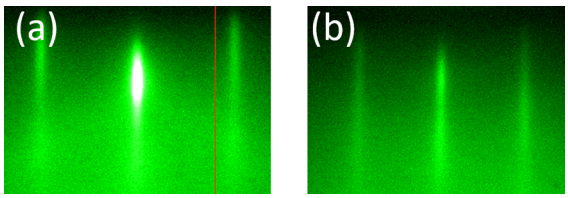

FIG. 6. RHEED image after InGaN growth of (a) sample A, (b) sample B.

APPENDIX B

STEM-HAADF image recorded over a larger area on sample A (Fig. 7) showed a sharp interface and InGaN/GaN SL structure with high structural quality.

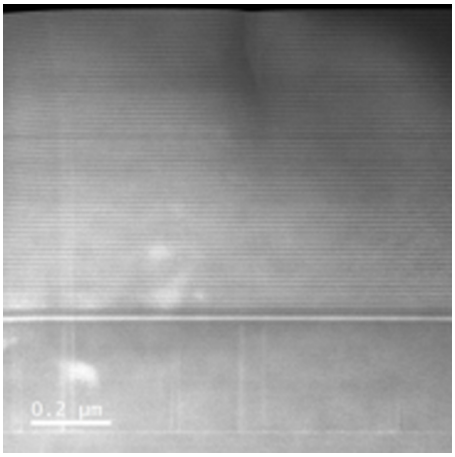

FIG. 7. STEM-HAADF image of sample A over a large area showing a sharp GaN and InGaN interface and a superlattice structure with high structural quality.

APPENDIX C

The SAED pattern recorded on sample A (Fig. 8) only has very sharp ordered diffraction spots from the crystal, suggesting that InGaN layers in the SASL structure are not ordered.

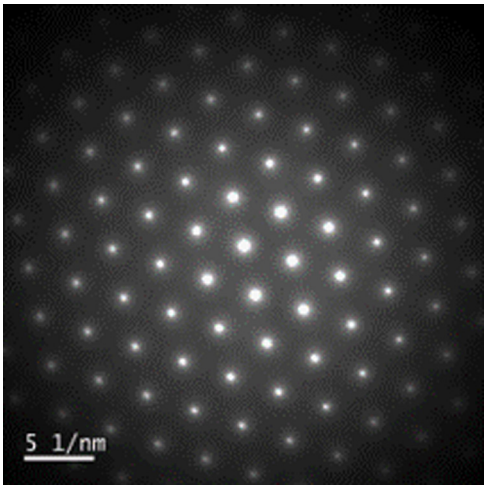

FIG. 8. SAED pattern taken from sample A along [0001] direction.

APPENDIX D

The SASL was absent in the InGaN film grown at 560 °C, as revealed by STEM-HAADF image (Fig. 9).

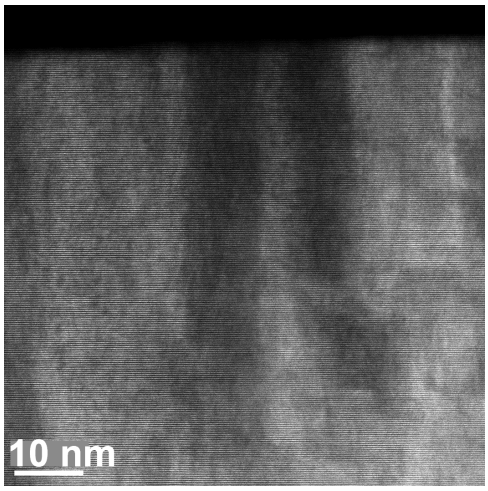

FIG. 9. STEM-HAADF image of $In_{0.25}Ga_{0.75}N$ film grown on GaN at 560 °C.

[1] S. Nakamura, M. Senoh, S. Nagahama, N. Iwasa, T. Yamada, T. Matsushita, A. Hiroyuki Kiyoku, and Y. Sugimoto, Characteristics of InGaN multi-quantum- well-structure laser diodes, Appl. Phys. Lett. **68**, 3269 (1996).

[2] S. Nakamura, M. Senoh, S. Nagahama, N. Iwasa, T. Yamada, T. Matsushita, Y. Sugimoto, and H. Kiyoku, Room-temperature continuous-wave operation of InGaN multi-quantum-well structure laser diodes with a lifetime of 27 hours, Appl. Phys. Lett. **70**, 1417 (1997).

[3] S. Nakamura, M. Senoh, S. I. Nagahama, N. Iwasa, T. Yamada, T. Matshushita, H. Kiyoku, and Y. Sugimoto, InGaN-based multi-quantum-well-structure laser diodes, Jpn. J. Appl. Phys. **35**, L74 (1997).

[4] S. P. DenBaars, D. Feezell, K. Kelchner, S. Pimputkar, C.-C. Pan, C.-C. Yen, S. Tanaka, Y. Zhao, N. Pfaff, R. Farrell, M. Iza, S. Keller, U. Mishra, J. S. Speck, and S. Nakamura, Development of gallium-nitride-based light-emitting diodes (LEDs) and laser diodes for energy-efficient lighting and displays, Acta Mater. **61**, 945 (2013).

[5] A. Chakraborty, B. A. Haskell, S. Keller, J. S. Speck, S. P. Denbaars, S. Nakamura, and U. K. Mishra, demonstration of nonpolar m-Plane InGaN/GaN light-emitting diodes on free-standing m-plane GaN substrates, Jpn. J. Appl. Phys., Part 2: Lett. **44**, L173 (2005).

[6] S. Pimputkar, J. S. Speck, S. P. DenBaars, and S. Nakamura, Prospects for LED lighting, Nat. Photonics **3**, 180 (2009).

[7] Y. Z. Chiou, Y. K. Su, S. J. Chang, J. Gong, Y. C. Lin, S. H. Liu, and C. S. Chang, High detectivity InGaN-GaN multiquantum well p-n junction photodiodes, IEEE J. Quantum Electron. **39**, 681 (2003).

[8] E. Muñoz, (Al,In,Ga)N-based photodetectors. Some materials issues, Phys. Status Solidi B: Basic Res. **244**, 2859 (2007).

[9] R. Dahal, B. Pantha, J. Li, J. Y. Lin, and H. X. Jiang, InGaN/GaN multiple quantum well solar cells with long operating wavelengths, Appl. Phys. Lett. **94**, 063505 (2009).

[10] O. Jani, I. Ferguson, C. Honsberg, and S. Kurtz, Design and characterization of GaNInGaN solar cells, Appl. Phys. Lett. **91**, 132117 (2007).

[11] J. Wu, W. Walukiewicz, K. M. Yu, W. Shan, J. W. Ager, E. E. Haller, H. Lu, W. J. Schaff, W. K. Metzger, and S. Kurtz, Superior radiation resistance of In 1-XGa XN Alloys: Full-solar-spectrum photovoltaic material system, J. Appl. Phys. **94**, 6477 (2003).

[12] C. Zhou, A. Ghods, V. G. Saravade, P. V. Patel, K. L. Yunghans, C. Ferguson, Y. Feng, B. Kucukgok, N. Lu, and I. T. Ferguson, Review—The current and emerging applications of the III-Nitrides, ECS J. Solid State Sci. Technol. **6**, Q149 (2017).

[13] K. Hestroffer, C. Lund, O. Koksaldi, H. Li, G. Schmidt, M. Trippel, P. Veit, F. Bertram, N. Lu, Q. Wang, J. Christen, M. J. Kim, U. K. Mishra, and S. Keller, Compositionally graded InGaN layers grown on vicinal N-face GaN substrates by plasma-assisted molecular beam epitaxy, J. Cryst. Growth **465**, 55 (2017).

[14] K. Hestroffer, F. Wu, H. Li, C. Lund, S. Keller, J. S. Speck, and U. K. Mishra, Relaxed c-plane InGaN layers for the growth of strain-reduced InGaN quantum wells, Semicond. Sci. Technol. **30**, 105015 (2015).

[15] A. M. Fischer, Y. O. Wei, F. A. Ponce, M. Moseley, B. Gunning, and W. A. Doolittle, Highly luminescent, high-indium-content InGaN film with uniform composition and full misfit-strain relaxation, Appl. Phys. Lett. **103**, 131101 (2013).

[16] M. Moseley, J. Lowder, D. Billingsley, and W. A. Doolittle, Control of surface adatom kinetics for the growth of high-indium content InGaN throughout the miscibility gap, Appl. Phys. Lett. **97**, 191902 (2010).

[17] Z. Xing, W. Yang, Z. Yuan, X. Li, Y. Wu, J. Long, S. Jin, Y. Zhao, T. Liu, L. Bian, S. Lu, and M. Luo, Growth and characterization of high in-content InGaN grown by MBE using metal modulated epitaxy technique (MME), J. Cryst. Growth **516**, 57 (2019).

[18] S. Valdueza-Felip, E. Bellet-Amalric, A. Núñez-Cascajero, Y. Wang, M.-P. Chauvat, P. Ruterana, S. Pouget, K. Lorenz, E. Alves, and E. Monroy, High In-content InGaN layers synthesized by plasma-assisted molecular-beam epitaxy: Growth conditions, strain relaxation, and In incorporation kinetics, J. Appl. Phys. **116**, 233504 (2014).

[19] D. Holec, P. M. F. J. Costa, M. J. Kappers, and C. J. Humphreys, Critical thickness calculations for InGaN/GaN, J. Cryst. Growth **303**, 314 (2007).

[20] T. Tao, Z. Zhang, L. Liu, H. Su, Z. Xie, R. Zhang, B. Liu, X. Xiu, Y. Li, P. Han, Y. Shi, and Y. Zheng, Surface morphology and composition studies in InGaN/GaN film grown by MOCVD, J. Semicond. **32**, 083002 (2011).

[21] N. Sharma, P. Thomas, D. Tricker, and C. Humphreys, Chemical mapping and formation of V-defects in InGaN multiple quantum wells, Appl. Phys. Lett. **77**, 1274 (2000).

[22] T. Egawa, B. Zhang, and H. Ishikawa, High performance of InGaN LEDs on (111) silicon substrates grown by MOCVD, IEEE Electron Device Lett. **26**, 169 (2005).

[23] F. C. P. Massabuau, S. L. Sahonta, L. Trinh-Xuan, S. Rhode, T. J. Puchtler, M. J. Kappers, C. J. Humphreys, and R. A. Oliver, Morphological, structural, and emission characterization of trench defects in InGaN/GaN quantum well structures, Appl. Phys. Lett. **101**, 212107 (2012).

[24] T. Schulz, L. Lymperakis, M. Anikeeva, M. Siekacz, P. Wolny, T. Markurt, and M. Albrecht, Influence of strain on the indium incorporation in (0001) GaN, Phys. Rev. Materials **4**, 073404 (2020).

[25] B. Jahnen, M. Albrecht, W. Dorsch, S. Christiansen, H. P. Strunk, D. Hanser, and R. F. Davis, Pinholes, dislocations and strain relaxation in InGaN, MRS Internet J. Nitride Semicond. Res. **3**, 39 (1998).

[26] S. Srinivasan, L. Geng, R. Liu, F. A. Ponce, Y. Narukawa, and S. Tanaka, Slip systems and misfit dislocations in InGaN epilayers, Appl. Phys. Lett. **83**, 5187 (2003).

[27] J. Mei, R. Liu, F. A. Ponce, H. Omiya, and T. Mukai, Basal-plane slip in InGaNGaN heterostructures in the presence of threading dislocations, Appl. Phys. Lett. **90**, 171922 (2007).

[28] R. Liu, J. Mei, S. Srinivasan, F. A. Ponce, H. Omiya, Y. Narukawa, and T. Mukai, Generation of misfit dislocations by basal-plane slip in InGaN/GaN heterostructures, Appl. Phys. Lett. **89**, 201911 (2006).

[29] Z. H. Wu, Y. Kawai, Y. Y. Fang, C. Q. Chen, H. Kondo, M. Hori, Y. Honda, M. Yamaguchi, and H. Amano, Spontaneous formation of highly regular superlattice structure in InGaN epilayers grown by molecular beam epitaxy, Appl. Phys. Lett. **98**, 141905 (2011).

[30] I. T. Ferguson, A. G. Norman, B. A. Joyce, T. Y. Seong, G. R. Booker, R. H. Thomas, C. C. Phillips, and R. A. Stradling, Molecular beam epitaxial growth of InAsSb strained layer superlattices. Can nature do it better? Appl. Phys. Lett. **59**, 3324 (1991).

[31] N. A. El-Masry, M. K. Behbehani, S. F. LeBoeuf, M. E. Aumer, J. C. Roberts, and S. M. Bedair, Self-assembled AlInGaN quaternary superlattice structures, Appl. Phys. Lett. **79**, 1616 (2001).

[32] L. K. Teles, M. Marques, L. M. R. Scolfaro, J. R. Leite, and L. G. Ferreira, Phase separation and ordering in Group-III nitride alloys, Braz. J. Phys. **34**, 593 (2004).

[33] M. K. Behbehani, E. L. Piner, S. X. Liu, N. A. El-Masry, and S. M. Bedair, Phase separation and ordering coexisting in InxGa1−xN grown by metal organic chemical vapor deposition, Appl. Phys. Lett. **75**, 2202 (1999).

[34] M. Gao, S. T. Bradley, Y. Cao, D. Jena, Y. Lin, S. A. Ringel, J. Hwang, W. J. Schaff, and L. J. Brillson, Compositional modulation and optical emission in AlGaN epitaxial films, J. Appl. Phys. **100**, 103512 (2006).

[35] J. E. Northrup, L. T. Romano, and J. Neugebauer, Surface energetics, pit formation, and chemical ordering in InGaN alloys, Appl. Phys. Lett. **74**, 2319 (1999).

[36] J. E. Northrup, GaN and InGaN(1122) surfaces: Group-III adlayers and indium incorporation, Appl. Phys. Lett. **95**, 133107 (2009).

[37] A. G. Norman, T.-Y. Seong, I. T. Ferguson, G. R. Booker, and B. A. Joyce, Structural studies of natural superlattices in Group III-V alloy epitaxial layers, Semicond. Sci. Technol. **8**, S9 (1993).

[38] X. T. Zheng, T. Wang, P. Wang, X. X. Sun, D. Wang, Z. Y. Chen, P. Quach, Y. X. Wang, X. L. Yang, F. J. Xu, Z. X. Qin, T. J. Yu, W. K. Ge, B. Shen, and X. Q. Wang, Full-composition-graded InxGa1-XN films grown by molecular beam epitaxy, Appl. Phys. Lett. **117**, 182101 (2020).

[39] S. W. Kaun, M. H. Wong, U. K. Mishra, and J. S. Speck, Molecular beam epitaxy for high-performance Ga-face GaN electron devices related content N-polar GaN epitaxy and high electron mobility transistors, Semicond. Sci. Technol **28**, 74001 (2013).

[40] K. Khan, M. Biswas, and E. Ahmadi, Growth of high quality (In,Ga)N films on O-face ZnO substrates by plasma-assisted molecular beam epitaxy, AIP Adv. **10**, 075120 (2020).

[41] B. Heying, E. J. Tarsa, C. R. Elsass, P. Fini, S. P. DenBaars, and J. S. Speck, Dislocation mediated surface morphology of GaN, J. Appl. Phys. **85**, 6470 (1999).

[42] K. Hestroffer, C. Lund, H. Li, S. Keller, J. S. Speck, and U. K. Mishra, Plasma-assisted molecular beam epitaxy growth diagram of InGaN on (0001)GaN for the optimized synthesis of InGaN compositional grades, Phys. Status Solidi Basic Res. **253**, 626 (2016).

[43] E. Iliopoulos, K. F. Ludwig, and T. D. Moustakas, Complex ordering in ternary wurtzite nitride alloys, J. Phys. Chem. Solids **64**, 1525 (2003).

[44] E. Iliopoulos, K. F. Ludwig, T. D. Moustakas, P. Komninou, T. Karakostas, G. Nouet, and S. N. G. Chu, Epitaxial growth and self-organized superlattice structures in AlGaN films grown by plasma assisted molecular beam epitaxy, Mater. Sci. Eng. B **87**, 227 (2001).

[45] M. Leyer, J. Stellmach, C. Meissner, M. Pristovsek, and M. Kneissl, The critical thickness of InGaN on (0 0 0 1)GaN, J. Cryst. Growth **310**, 4913 (2008).

[46] D. Holec, Y. Zhang, D. V. S. Rao, M. J. Kappers, C. McAleese, and C. J. Humphreys, Equilibrium critical thickness for misfit dislocations in III-Nitrides, J. Appl. Phys. **104**, 123514 (2008).

[47] E. Ertekin, P. A. Greaney, and D. C. Chrzan, Equilibrium limits of coherency in strained nanowire heterostructures, J. Appl. Phys **97**, 114325 (2005).

[48] T. Stankevič, D. Dzhigaev, and Z. Bi, Strain mapping in an InGaN/GaN nanowire using a nano-focused x-ray beam, Appl. Phys. Lett **107**, 103101 (2015).

[49] C.-K. Sun, T.-L. Chiu, S. Keller, G. Wang, M. S. Minsky, S. P. DenBaars, and J. E. Bowers, Time-resolved photoluminescence studies of InGaN/GaN single-quantum-wells at room temperature, Appl. Phys. Lett. **71**, 425 (1998).

[50] P. Lefebvre, A. Morel, M. Gallart, T. Taliercio, J. Allègre, B. Gil, H. Mathieu, B. Damilano, N. Grandjean, and J. Massies, High internal electric field in a graded-width InGaN/GaN quantum well: Accurate determination by time-resolved photoluminescence spectroscopy, Appl. Phys. Lett. **78**, 1252 (2001).

[51] M. Takeguchi, M. R. McCartney, and D. J. Smith, Mapping in concentration, strain, and internal electric field in InGaN/GaN quantum well structure, Appl. Phys. Lett. **84**, 2103 (2004).

[52] M. S. Minsky, S. B. Fleischer, A. C. Abare, J. E. Bowers, E. L. Hu, S. Keller, and S. P. Denbaars, Characterization of high-quality InGaN/GaN multiquantum wells with time-resolved photoluminescence, Appl. Phys. Lett. **72**, 1066 (1998).

[53] M. Pophristic, F. H. Long, C. Tran, I. T. Ferguson, and R. F. Karlicek, Time-resolved photoluminescence measurements of quantum dots in InGaN multiple quantum wells and light-emitting diodes, J. Appl. Phys. **86**, 1114 (1999).

[54] A. D. Kurtz, S. A. Kulin, and B. L. Averbach, Effect of dislocations on the minority carrier lifetime in semiconductors, Phys. Rev. **101**, 1285 (1956).

[55] J. S. Im, H. Kollmer, J. Off, A. Sohmer, F. Scholz, and A. Hangleiter, Reduction of oscillator strength due to piezoelectric fields in $GaN/Al_xGa_{1-x}N$ quantum wells, Phys. Rev. B **57**, R9435 (1998).

[56] E. Berkowicz, D. Gershoni, G. Bahir, E. Lakin, D. Shilo, E. Zolotoyabko, A. C. Abare, S. P. Denbaars, and L. A. Coldren, Measured and calculated radiative lifetime and optical absorption of quantum structures, Phys. Rev. B **61**, 10994 (2000).